Simulation of a Three-Phase Transformer Using an Improved Anisotropy Model

Hans Vande Sande, Tim Boonen, Ioan Podoleanu, François Henrotte, and Kay Hameyer, *Senior Member, IEEE*

***Abstract*—The nonlinear and anisotropic behavior of grain-oriented ferromagnetic materials enters numerical field computations via the reluctivity tensor. In this paper, an improved reluctivity tensor model is discussed. It is pointed out in which way this model is integrated in a Newton iterative solver. However, to retain the attractive properties of the conjugate gradient algorithm, it is required to modify the definition of the Jacobian matrix. Several simulations of a three-phase transformer are performed and compared, in order to demonstrate the properties of the reluctivity model and the proposed Newton solver.**

***Index Terms*—Anisotropic media, magnetostatics, nonlinear magnetics.**

I. Introduction

NONLINEAR magnetostatic systems are described by

$$\nabla \times (\nu \nabla \times \vec{A}) = \vec{J} \tag{1}$$

where $\vec{A}$ is the vector potential [Vs/m], $\vec{J}$ the applied current density vector [A/m^2] and ν the reluctivity tensor [Am/Vs]. This tensor relates the flux density $\vec{B} = \nabla \times \vec{A}$ [Vs/m^2] to the field strength $\vec{H}$ [A/m], according to

$$\vec{H} = \nu \vec{B}. \tag{2}$$

The nonlinearity of the problem is due to the dependence of ν on $\vec{A}$ via $\vec{B}$. For two-dimensional problems, such as the simulation of the field distribution in the laminations of the three-phase transformer being considered here, (1) simplifies into

$$\nabla \cdot (\nu' \nabla A_z) = -J_z \tag{3}$$

where A_z and J_z are the components of $\vec{A}$ and $\vec{J}$ that are perpendicular to the surface of the laminations and

$$\nu' = \begin{pmatrix} \nu_{yy} & -\nu_{yx} \\ -\nu_{xy} & \nu_{xx} \end{pmatrix} \tag{4}$$

Manuscript received July 1, 2003. This paper presents research results of the Belgian Fund for Scientific Research and the Belgian programme on Interuniversity Poles of Attraction initiated by the Belgian State, Prime Minister's Office, Science Policy Programming.

H. Vande Sande is with the Flanders' Mechatronics Technology Centre, B-3001 Leuven, Belgium (e-mail: hans.vandesande@fmtc.be).

T. Boonen is with the Department of Computer Science, Katholieke Universiteit Leuven, B-3001 Leuven, Belgium (e-mail: tim.boonen@cs.kuleuven.ac.be).

I. Podoleanu and F. Henrotte are with the Department of ESAT, Katholieke Universiteit Leuven, B-3001 Leuven, Belgium (e-mail: francois.henrotte@esat.kuleuven.ac.be).

K. Hameyer is with the Institut für Elektrische Machinen (IEM), Rheinisch-Westfälische Technische Hochschule Aachen, D-52056 Aachen, Germany (e-mail: Kay.Hameyer@iem.RWTH-Aachen.de).

Digital Object Identifier 10.1109/TMAG.2004.825004

is a reordering of the reluctivity tensor

$$\nu = \begin{pmatrix} \nu_{xx} & \nu_{xy} \\ \nu_{yx} & \nu_{yy} \end{pmatrix} \tag{5}$$

relating $\vec{H}$ and $\vec{B}$ in the global coordinate system $\{x, y\}$. This paper discusses techniques for solving (3), where the entries of ν are determined from an improved anisotropy model.

II. Reluctivity Tensor Properties

It is assumed that the second-rank tensor ν is symmetric, i.e., $\nu_{xy} = \nu_{yx}$, and positive definite. This implies that all magnetic processes taking place at the microscopic level are thermodynamically reversible [1]. As a consequence, magnetic hysteresis effects are not treated in the analysis. The value of the tensor entries depends on the coordinate system in which the magnetic properties are considered. It is possible to determine a *principal coordinate system* $\{p, q\}$ for which the off-diagonal tensor entries are zero and the diagonal entries are positive [2]. Hence, the reluctivity tensor contains only two independent entries.

For magnetically isotropic materials, $\nu_{xx} = \nu_{yy}$ and $\nu_{xy} = \nu_{yx} = 0$. The axes p and q coincide with the material axes for which $\vec{B}$ is parallel to $\vec{H}$. Due to the Goss-texture of most grain-oriented steels used in the laminated cores of large transformers, $\vec{B}$ and $\vec{H}$ are generally in parallel to the rolling direction (rd) and the transverse direction (td) of the steel sheet [3]–[6]. Therefore, the entries of the reluctivity tensor, when considered in the coordinate system $\{p, q\}$, are denoted by ν_{rd} and ν_{td} (Fig. 1).

In order to evaluate ν in the global coordinate system $\{x, y\}$, ν_{rd} and $= \nu_{\mathrm{td}}$ are first determined. Next, the tensor transformation rule is used [1]

$$\begin{pmatrix} \nu_{xx} & \nu_{xy} \\ \nu_{yx} & \nu_{yy} \end{pmatrix} = \mathbf{T}^{-1} \begin{pmatrix} \nu_{\mathrm{rd}} & 0 \\ 0 & \nu_{\mathrm{td}} \end{pmatrix} \mathbf{T} \tag{6}$$

where

$$\mathbf{T} = \begin{pmatrix} \cos\phi & \sin\phi \\ -\sin\phi & \cos\phi \end{pmatrix} \tag{7}$$

is the matrix of direction cosines and ϕ is the angle between the x axis and the p axis (// rd). Below, the field-dependent behavior of ν_{rd} and ν_{td} is discussed.

III. Reluctivity Tensor Model

When a field $\vec{H}$ is applied to a grain-oriented silicon steel sheet, the ferromagnetic material is magnetized. The resulting flux density is $\vec{B}$ [7], [8]. The direction β (relative to the rolling

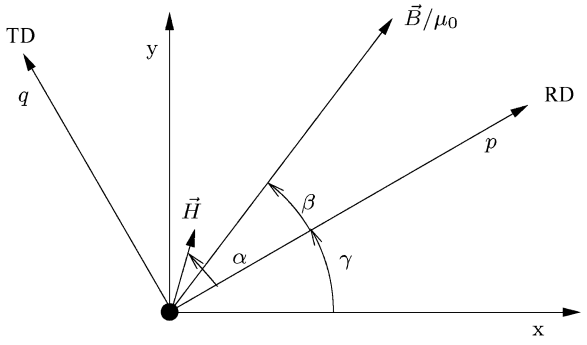

Fig. 1. Graphical interpretation of the relation between $\vec{H}$ and $\vec{B}$, with definition of their respective angles α and β relative to the principal coordinate system $\{p, q\}$ of the reluctivity tensor. The rolling and transverse direction are parallel to the p and q axis, respectively. They are rotated over an angle γ relative to the global x and y axis.

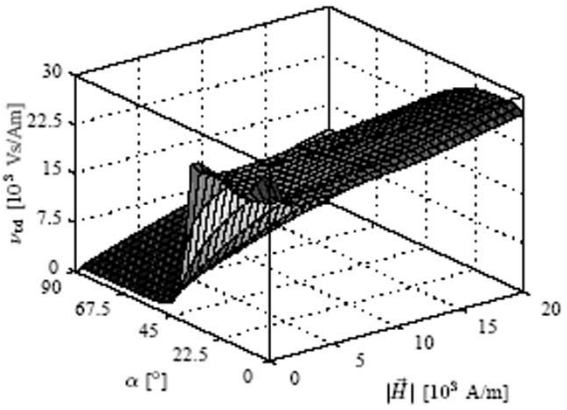

Fig. 3. Reluctivity ν_{td} in the transverse direction as a function of the direction α and the magnitude $|\vec{H}|$ of the applied field $\vec{H}$, for silicon iron FeSi3% having a Goss-texture.

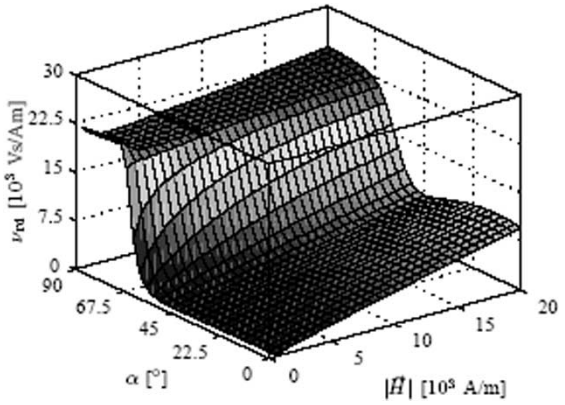

Fig. 2. Reluctivity ν_{rd} in the rolling direction as a function of the direction α and the magnitude $|\vec{H}|$ of the applied field $\vec{H}$, for silicon iron FeSi3% having a Goss-texture.

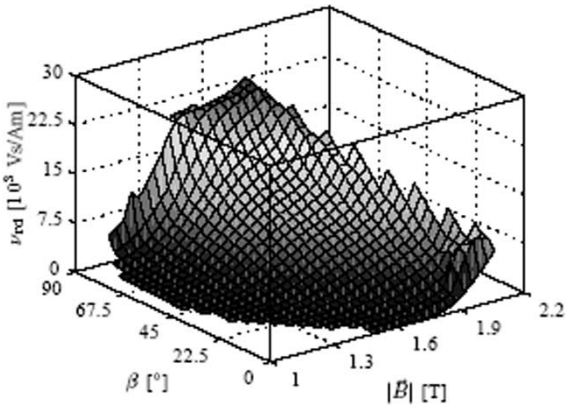

Fig. 4. Reluctivity ν_{rd} in the rolling direction as a function of the direction β and the magnitude $|\vec{B}|$ of the flux density, for silicon iron FeSi3% with a Goss-texture.

direction) and magnitude $|\vec{B}|$ of $\vec{B}$, both depend on the direction α and the magnitude $|\vec{H}|$ of $\vec{H}$ and the magnetic history of the material. Since hysteresis effects are not considered here, $\vec{B}$ is a nonlinear function of $\vec{H}$ with the additional property that $\vec{B}(-\vec{H}) = -\vec{B}(\vec{H})$. It follows that each pair $[\vec{H}, \vec{B}(\vec{H})]$ uniquely defines a value for ν_{rd} and ν_{td}, both depending on α and $|\vec{H}|$. In [9] and [10], it is described in which way expressions can be obtained for ν_{rd} and ν_{td}, by combining magnetization measurements with a physical anisotropy model for Goss-textured silicon iron. The results are plotted in Figs. 2 and 3. It is remarked that this model only holds for field strengths at which the coherent rotation process predominates, i.e., at field strengths that saturate the ferromagnetic material.

The flux density can be obtained from a finite-element solution of (3), using $\vec{B} = \nabla \times \vec{A}$. As a consequence, in order to determine the reluctivity tensor from such a solution, one needs a representation of ν_{rd} and ν_{td} as a function of the direction β and magnitude $|\vec{B}|$ of $\vec{B}$. By appropriately transforming Figs. 2 and 3, Figs. 4 and 5 are obtained. Obviously, a large part of the $|\vec{B}| - \beta$ region is not covered by this model, since the model only holds in the saturation region. To overcome this problem, a well-considered extrapolation is carried out. The goal of this extrapolation is to dispose of a reluctivity tensor model which allows to do numerical simulations. Alternatively, additional measurements could be done for improving the quality of the final model. The extrapolation is performed as follows.

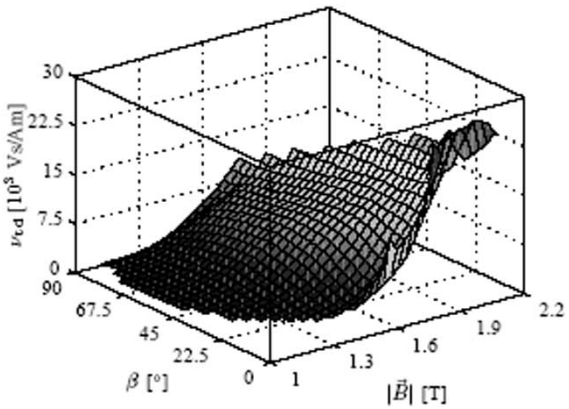

Fig. 5. Reluctivity ν_{td} in the transverse direction as a function of the direction β and the magnitude $|\vec{B}|$ of the flux density, for silicon iron FeSi3% with a Goss-texture.

- At high flux densities, it is suggested to extrapolate ν_{rd} and ν_{td} linearly. Theoretically, if $|\vec{B}|$ is very large, this could yield reluctivity values that exceed the reluctivity of air. However, this situation is irrealistic in the final solution of a nonlinear problem.

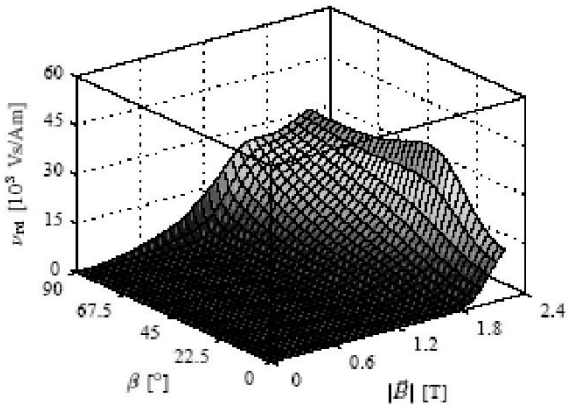

Fig. 6. Modeled reluctivity ν_{rd} in the rolling direction as a function of the direction β and the magnitude $|\vec{B}|$ of the flux density, for silicon iron FeSi3% with a Goss-texture.

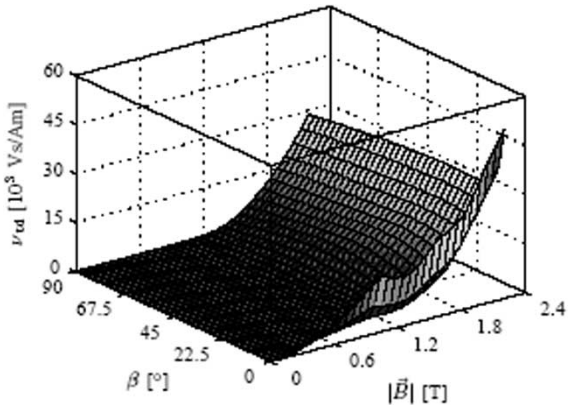

Fig. 7. Modeled reluctivity ν_{td} in the transverse direction as a function of the direction β and the magnitude $|\vec{B}|$ of the flux density, for silicon iron FeSi3% with a Goss-texture.

- At low flux densities, it is remarked that the measured magnetization curves in the rolling and transverse direction appear in Figs. 4 and 5 at $\beta = 0°$ and $90°$, respectively, i.e., $\nu_{\mathrm{rd}}(|\vec{B}|, 0°)$ and $\nu_{\mathrm{td}}(|\vec{B}|, 90°)$. Their behavior at low flux densities is known. Moreover, measurements with rotational single sheet testers (RSST) reveal that the $\vec{H}$-locus becomes more and more elliptically shaped if the magnitude of a circular $\vec{B}$-locus decreases. Such a behavior can be described with a tensor whose components are independent of the angle β of $\vec{B}$. For these reasons, it is suggested to extrapolate $\nu_{\mathrm{rd}}(|\vec{B}|, \beta)$ and $\nu_{\mathrm{td}}(|\vec{B}|, \beta)$ proportionally to the known $\nu_{\mathrm{rd}}(|\vec{B}|, 0°)$ and $\nu_{\mathrm{td}}(|\vec{B}|, 90°)$, in such a way that for $|\vec{B}|$ smaller than a predefined limit, $\nu_{\mathrm{rd}}(|\vec{B}|, \beta) = \nu_{\mathrm{rd}}(|\vec{B}|, 0°)$ and $\nu_{\mathrm{td}}(|\vec{B}|, \beta) = \nu_{\mathrm{td}}(|\vec{B}|, 90°)$.

The resulting reluctivity tensor model is plotted in Figs. 6 and 7.

IV. Nonlinear Solving Process

For solving (3) by the finite-element method, the domain of the problem is divided into triangles. The discretized magnetic vector potential writes

$$A_z(\mathbf{x}) = \sum_{i=1}^{n} A_{zi}\varphi_i(\mathbf{x}) \tag{8}$$

where n is the number of nodes and φ_i the corresponding shape functions. Here, linear shape functions are applied. Galerkin's method yields the following system of algebraic equations:

$$\mathbf{r}(\mathbf{A}) = \mathbf{K}(\mathbf{A})\mathbf{A} - \mathbf{T} = \mathbf{0} \tag{9}$$

where $\mathbf{r}$ is the residual vector, $\mathbf{K}$ the stiffness matrix, vector $\mathbf{A}$ the vector potentials in the nodes of the mesh, and $\mathbf{T}$ the vector representing the applied current sources. If only one element is considered, $\mathbf{K} = \mathbf{K}^{(\mathrm{e})}$ is a (3×3) matrix, whose entries are given by

$$\mathbf{K}_{ij}^{(\mathrm{e})} = \frac{1}{4\Delta}(b_i \quad c_i)\nu'\begin{pmatrix} b_j \\ c_j \end{pmatrix} \tag{10}$$

where Δ is the area of the element, $b_1 = y_2 - y_3, \cdots, c_1 = x_3 - x_2, \cdots$ [11]. The stiffness matrix of the complete problem is obtained by assembling the entries of $\mathbf{K}^{(\mathrm{e})}$ in $\mathbf{K}$, taking into account possible boundary conditions [12]. It can be shown that the obtained $(n \times n)$ matrix $\mathbf{K}$ is symmetric and positive-definite, provided ν_{rd} and ν_{td} are positive [13]. Obviously, the latter condition is always true. The nonlinearity of the problem is due to the dependency of $\mathbf{K}$ on $\mathbf{A}$ via the reluctivity tensor. Equation (9) represents a system of nonlinear equations.

For practical problems, the numerical solution of (9) requires an iterative approach. Starting from an initial guess, $\mathbf{A}$ is steadily updated until the norm of the residual is sufficiently small. At each iteration, the system

$$\mathbf{J}\mathbf{d} = -\mathbf{r} \tag{11}$$

must be solved, with $\mathbf{J}$ the Jacobian of the residual (or its approximation) and $\mathbf{d}$ a direction. In computational magnetics, it is common to update $\mathbf{A}$ with a line search procedure along that direction [14], [15]. Alternatively, a trust region procedure can be used, in which $\mathbf{d}$ may be different from the exact solution of (11) [16]. In this paper, they are both used as a tool. A thorough discussion and comparison of these techniques is given in [17].

The convergence properties of line search and trust region methods depends on the accuracy with which the Jacobian is determined. Three cases can be distinguished.

- **Linear convergence** is obtained by setting $\mathbf{J} = \mathbf{I}$. The direction $\mathbf{d}$ is the steepest descent direction.
- **Superlinear convergence** is obtained by setting $\mathbf{J}$ to an approximation of the Jacobian, yielding a *quasi-Newton method*. From (9), it follows that $\mathbf{J} = \mathbf{K}$ is the most appropriate choice here, since no additional computations must be performed for its evaluation. In that case, the method is better known as *Picard method* or *successive substitution method*.
- **Quadratic convergence** is obtained by setting $\mathbf{J} = \nabla\mathbf{r}$, yielding the so-called *Newton method*.

When considering one single finite element, the entries of the Jacobian $\mathbf{J} = \mathbf{J}^{(\mathrm{e})}$ are defined by

$$\mathbf{J}_{ij}^{(\mathrm{e})} = \frac{\partial \mathbf{r}_i^{(\mathrm{e})}}{\partial \mathbf{A}_j^{(\mathrm{e})}} \tag{12}$$

$$= \mathbf{K}_{ij}^{(\mathrm{e})} + \sum_{k=1}^{3} \frac{\partial \mathbf{K}_{ik}^{(\mathrm{e})}}{\partial \mathbf{A}_j^{(\mathrm{e})}} \mathrm{A}_k^{(\mathrm{e})}. \tag{13}$$

Hence, the Jacobian equals the sum of the stiffness matrix and a matrix that contains derivative information. Since the reluctivity tensor depends on two parameters, $|\vec{B}|$ (or $B^2 = |\vec{B}|^2$) and β, this additional matrix is the sum of two submatrices itself

$$\mathbf{J}^{(\mathrm{e})} = \mathbf{K}^{(\mathrm{e})} + \mathbf{M}^{(\mathrm{e})} + \mathbf{N}^{(\mathrm{e})} \tag{14}$$

with

$$\mathbf{M}^{(\mathrm{e})} = \frac{2}{\Delta}\left(\mathbf{Q}^{(\mathrm{e})}\mathbf{A}^{(\mathrm{e})}\right).\left(\mathbf{P}^{(\mathrm{e})}\mathbf{A}^{(\mathrm{e})}\right)^{\mathrm{T}} \tag{15}$$

$$\mathbf{N}^{(\mathrm{e})} = \frac{1}{B^2\Delta}\left(\mathbf{S}^{(\mathrm{e})}\mathbf{A}^{(\mathrm{e})}\right).\left(\mathbf{R}^{(\mathrm{e})}\mathbf{A}^{(\mathrm{e})}\right)^{\mathrm{T}} \tag{16}$$

and

$$\mathbf{P}_{ij}^{(\mathrm{e})} = \frac{1}{4\Delta}(b_i \quad c_i)\begin{pmatrix} b_j \\ c_j \end{pmatrix} \tag{17}$$

$$\mathbf{Q}_{ij}^{(\mathrm{e})} = \frac{1}{4\Delta}(b_i \quad c_i)\frac{\partial \nu'}{\partial B^2}\begin{pmatrix} b_j \\ c_j \end{pmatrix} \tag{18}$$

$$\mathbf{R}_{ij}^{(\mathrm{e})} = \frac{1}{4\Delta}(b_i \quad c_i)\begin{pmatrix} -c_j \\ b_j \end{pmatrix} \tag{19}$$

$$\mathbf{S}_{ij}^{(\mathrm{e})} = \frac{1}{4\Delta}(b_i \quad c_i)\frac{\partial \nu'}{\partial \beta}\begin{pmatrix} b_j \\ c_j \end{pmatrix}. \tag{20}$$

As for ν', the partial derivatives in (18) and (20) depend on $|\vec{B}|$ (or B^2) and β. For the particular case the material under consideration is magnetically nonlinear and isotropic, the reluctivity tensor may be replaced by a scalar ν and the elementary Jacobian reduces to the well-known form [11]

$$\mathbf{J}^{(\mathrm{e})} = \mathbf{K}^{(\mathrm{e})} + \frac{2}{\Delta}\frac{\mathrm{d}\nu}{\mathrm{d}B^2}\left(\mathbf{P}^{(\mathrm{e})}\mathbf{A}^{(\mathrm{e})}\right).\left(\mathbf{P}^{(\mathrm{e})}\mathbf{A}^{(\mathrm{e})}\right)^{\mathrm{T}}. \tag{21}$$

The total Jacobian matrix $\mathbf{J}$ is assembled in the same way as the stiffness matrix, with a special treatment of the boundary conditions [12]. At the end

$$\mathbf{J} = \mathbf{K} + \mathbf{M} + \mathbf{N} \tag{22}$$

is obtained.

From (17) to (20), one sees that $\mathbf{P}^{(\mathrm{e})}$, $\mathbf{Q}^{(\mathrm{e})}$, and $\mathbf{S}^{(\mathrm{e})}$ are symmetric matrices, whereas $\mathbf{R}^{(\mathrm{e})}$ is not. As a consequence, only $\mathbf{M}$ is symmetric. Additionally, if $\partial\nu_{\mathrm{rd}}/\partial B^2$ and $\partial\nu_{\mathrm{td}}/\partial B^2$ are positive, $\mathbf{M}$ is positive-definite as well [13]. Unfortunately, these partial derivatives might not be positive in the Rayleigh region of the magnetization curves [7], [8].

These observations are important for choosing an appropriate Krylov subspace method for solving (11). The conjugate gradient (CG) method is the ultimate solver for symmetric positive-definite systems of equations [18]. It can be used to solve the nonlinear problem by the Picard method. However, it is not possible to retain its attractive properties if the Newton method is desired, because $\mathbf{N}$ is not symmetric and the contribution of $\mathbf{M}$ may yield an indefinite Jacobian $\mathbf{J}$. Therefore, it is suggested to approximate $\mathbf{J}$ as follows:

$$\mathbf{J} \approx \mathbf{K} + \mathbf{M}^{\star} \tag{23}$$

where $\mathbf{M}^{\star}$ is computed according to (15), but without allowing negative values for $\partial\nu_{\mathrm{rd}}/\partial B^2$ and $\partial\nu_{\mathrm{td}}/\partial B^2$ in (18). In this way, the convergence of the nonlinear system is not quadratic anymore, but it is expected to be better when compared to the case in which $\mathbf{J}$ is approximated by $\mathbf{K}$. This method is called *simplified Newton method* in the text.

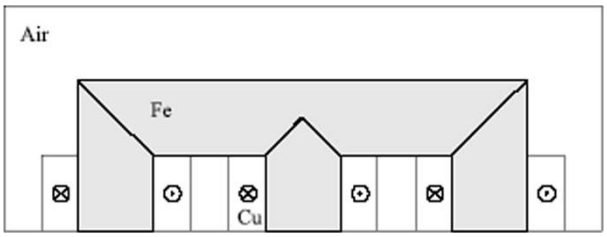

Fig. 8. Outline of the three-phase transformer under consideration. The grain orientation of the ferromagnetic laminations is vertical in the limbs and horizontal in the yokes.

Fig. 9. Flux line distribution obtained when the phase of the currents in the coils is $-85°$, $35°$, and $155°$, respectively. The flux density in the middle limb is approximately 1.58 T.

V. Simulation of a Three-Phase Transformer

The proposed techniques are now tested for the simulation of the no-load condition of a three-phase transformer plotted in Fig. 8. Due to symmetry, the other half must not be considered in the simulation. The bottom line is modeled as a homogeneous Neumann boundary, the remaining air boundary as a homogeneous Dirichlet boundary. The shape of the ferromagnetic regions is indicated on the figure. Their grain orientation is vertical in the limbs of the transformer and horizontal in the yokes. A three-phase current is applied to the three copper coils around each limb. Static solutions are computed for a series of time instants over one period of the applied current, whose amplitude drives the material into saturation.

A. Field Distribution

In Fig. 9, the flux line distribution is plotted for the case of phase of the currents in the coils is $-85°$, $35°$, and $155°$, respectively. The flux density in the middle limb is approximately 1.58 T. Obviously, the bending of the field lines occurs particularly near the joints. Moreover, due to the anisotropy, some flux lines tend to fan out significantly from the middle limb, although returning to the other yoke.

Fig. 10 shows some of the computed flux density loci in the joint-region between the middle limb and the yoke of the transformer. Rotational magnetization is predominant close the joints of the transformer, in contrast to the rest of the transformer where alternating magnetization prevails. In [19] and [20], similar $|\vec{B}|$-loci have been measured. Moreover, [19] cites that rotational fluxes occurs in approximately 25% of the square around

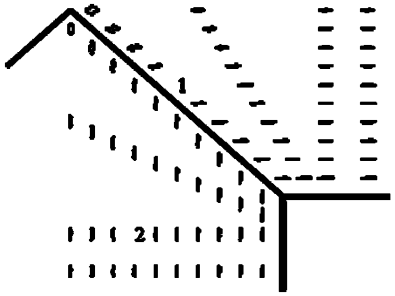

Fig. 10. Some flux density loci in the region close to the joint between the middle limb and the yoke of the transformer.

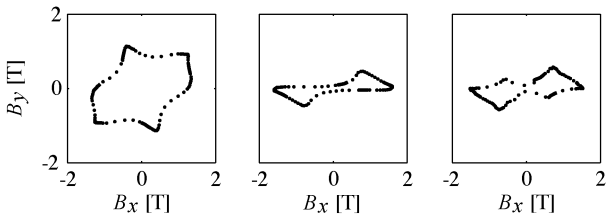

Fig. 11. Detail of the flux density loci in point 1 of Fig. 10, obtained when simulating with the isotropic model (left), the simplified anisotropic model (middle) and the improved anisotropy model (right).

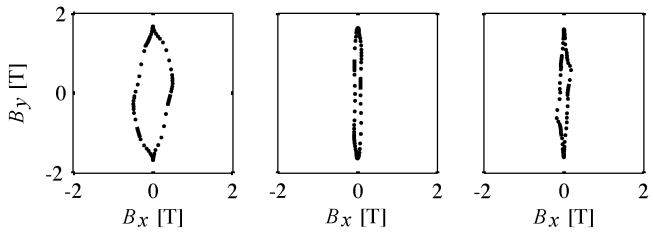

Fig. 12. Detail of the flux density loci in point 2 of Fig. 10, obtained when simulating with the isotropic model (left), the simplified anisotropic model (middle) and the improved anisotropy model (right).

the T-joint, where Fig. 10 reveals that it is approximately the same here.

Figs. 11 and 12 zoom in on the $|\vec{B}|$-loci in points 1 and 2 of Fig. 10, obtained when simulating with three different material models:

- at the right, the improved anisotropy model presented in this paper;
- in the middle, a simplified anisotropy model, obtained from the previous one by only considering the components of $\vec{B}$ along the rolling or transverse direction

$$\nu_{\rm rd} = \nu_{\rm rd}\left(|\vec{B}|\cos\beta, 0^\circ\right) \tag{24}$$

$$\nu_{\rm td} = \nu_{\rm td}\left(|\vec{B}|\sin\beta, 90^\circ\right); \tag{25}$$

- at the left, an isotropic model, obtained from the previous one by considering $|\vec{B}|$ along the rolling direction

$$\nu_{\rm rd} = \nu_{\rm rd}\left(|\vec{B}|, 0^\circ\right) \tag{26}$$

$$\nu_{\rm td} = \nu_{\rm rd}\left(|\vec{B}|, 0^\circ\right). \tag{27}$$

The sequence of dots on these loci represent the position of $\vec{B}$ at regular time intervals. It is concluded that the rotation of $\vec{B}$ does not appear to be smooth: $\vec{B}$ rather stays close to a certain direction for a while, although its magnitude may continuously change, before it suddenly rotates toward a new direction. Similar behavior is observed at other points close to the joints. The isotropic material model generally yields higher magnitudes of $\vec{B}$ in all directions, since the increased reluctivity in the transverse direction is never considered. The shape of the $\vec{B}$-locus obtained with both anisotropy models better resembles each other. From the $\vec{B}$-locus in point 1, it follows that the simplified anisotropy allows a larger average deviation of the flux lines from the preferred rolling direction.

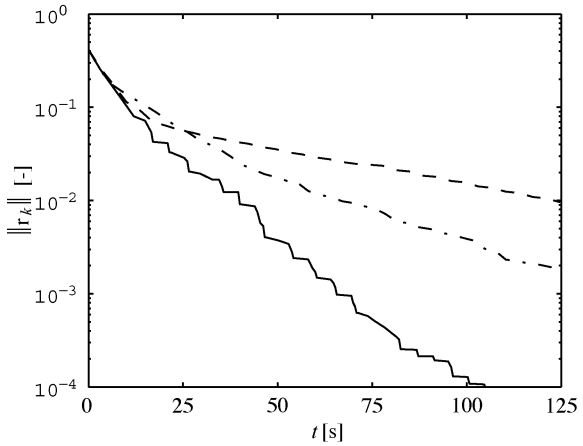

Fig. 13. Convergence of the Picard trust region method (solid), the Picard line search method with cubic line search (dashdotted) and the Picard line search method with backtracking line search (dashed).

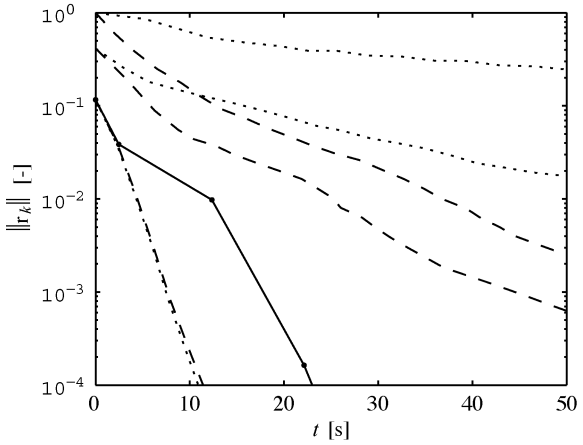

Fig. 14. Convergence of the Picard line search method (dotted) with the simplified Newton method (dashed), at three different current levels in the coils. The solid line indicates the deteriorating effect of allowing negative partial derivatives in the simplified Newton method.

B. Convergence

Fig. 13 compares the convergence of the Picard line search and trust region method. The convergence rate of the trust region method (solid) is higher than the one with cubic line search (dashdot) or even backtracking line search (dashed), in which the relaxation factor is successively divided by two [17]. The significantly higher convergence rate of the trust region approach in this example is a coincidence. However, the figure

illustrates the improvement that can be obtained by using a slightly more sophisticated line search algorithm.

In Fig. 14, the convergence of the Picard line search method (dotted) is compared with the convergence of the simplified Newton method (dashed), at three different current levels in the coils. The inclusion of derivative information in the evaluation of the (approximate) Jacobian, generally yields a significant improvement of the convergence rate, except when the flux density level in the device is low. In that case, a major part of the ferromagnetic material is operated in the Rayleigh region, where the derivative information is not retained. To show the deteriorating effect of these negative-valued partial derivatives on the convergence, the simulation is repeated, using the exact $\mathbf{M}$ in (23) (solid line). In some simulations at these low flux density levels, it was even impossible to solve the linear systems with the CG-algorithm, since the positive-definite requirement was violated.

VI. Conclusion

Grain-oriented ferromagnetic materials exhibit macroscopic anisotropy. As long as hysteresis is not considered, this anisotropy can be characterized by a symmetric and positive definite reluctivity tensor. A model which allows to evaluate the entries of this tensor, as a function of the magnitude and direction of the flux density, is discussed. In order to benefit from the convergence properties of the Newton solver, an analytical expression for the Jacobian is derived. However, a simplification is proposed to ensure the symmetric and positive definite requirements. It is shown that this has a limited impact on the solution process, since the convergence rate remains much higher than for the Picard solver.

References

[1] J. F. Nye, *Physical Properties of Crystals*, 2nd ed. Oxford, U.K.: Oxford Univ. Press, 1985.

[2] D. A. Danielson, *Vectors and Tensors in Engineering and Physics*, 2nd ed. Reading, MA: Addison-Wesley, 1997.

[3] J. Harase, R. Shimizu, and N. Takahashi, "Mechanism of Goss secondary recrystalization in grain-oriented silicon steel," *Textures Microstruct.*, vol. 14–18, pp. 679–684, 1991.

[4] U. F. Kocks, C. N. Tomé, and H. R. Wenk, *Texture and Anisotropy: Preferred Orientations in Polycrystals and Their Effect on Materials Properties*. Cambridge, UK: Cambridge Univ. Press, 1998.

[5] D. N. Lee and H. T. Jeong, "The evolution of Goss texture in silicon steel," *Scripta Mater.*, vol. 38, no. 8, pp. 1219–1223, 1998.

[6] M. Nakano, K. Ishiyama, K. I. Arai, and H. Fukunaga, "Relationship between rolling direction and texture in thin grain-oriented 3% silicon steel," *J. Magn. Magn. Mater.*, vol. 196–197, pp. 344–345, 1999.

[7] R. M. Bozorth, *Ferromagnetism*. Princeton, NJ: Van Nostrand, 1951.

[8] D. Jiles, *Introduction to Magnetism and Magnetic Materials*. London, U.K.: Chapman & Hall, 1991.

[9] H. Vande Sande, W. Deprez, F. Henrotte, K. Hameyer, and L. Froyen, "A hybrid statistical model of the anisotropy of Goss textured silicon steel," in *Proc. Int. Conf. Magnetism (ICM'03)*, Rome, Italy, July 2003.

[10] H. Vande Sande, F. Henrotte, L. Froyen, and K. Hameyer, "A hybrid method for determining the reluctivity tensor components of Goss textured ferromagnetic materials," *Int. J. Comput. Math. Elect. Electron. Eng.*, vol. 23, no. 2, 2004.

[11] P. P. Silvester and R. L. Ferrari, *Finite Elements for Electrical Engineers*, 2nd ed. Cambridge, U.K.: Cambridge Univ. Press, 1996.

[12] K. Hameyer and R. Belmans, *Numerical Modeling and Design of Electrical Machines and Devices*. Southampton, U.K.: WIT Press, 1999.

[13] A. Quarteroni and A. Valli, *Numerical Approximation of Partial Differential Equations*. Berlin, Germany: Springer-Verlag, 1994.

[14] K. Fujiwara, T. Nakata, and N. Okamoto, "Method for determining relaxation factor for modified Newton-Raphson method," *IEEE Trans. Magn.*, vol. 29, pp. 1962–1965, Mar. 1993.

[15] J. O'Dwyer and T. O'Donnell, "Choosing the relaxation parameter for the solution of nonlinear magnetic field problems by the Newton-Raphson method," *IEEE Trans. Magn.*, vol. 31, pp. 1484–1487, May 1995.

[16] H. Vande Sande, H. De Gersem, F. Henrotte, and K. Hameyer, "Solving nonlinear magnetic problems using Newton trust region methods," *IEEE Trans. Magn.*, vol. 39, pp. 1709–1712, May 2003.

[17] J. Nocedal and S. J. Wright, *Numerical Optimization*, 1st ed. New York: Springer, 1999, Springer Series in Operations Research.

[18] Y. Saad, *Iterative Methods for Sparse Linear Systems*. Boston, MA: PWS, 1996.

[19] A. J. Moses, "Comparison of transformer loss prediction from computed and measured flux density distribution," *IEEE Trans. Magn.*, vol. 34, pp. 1186–1188, July 1998.

[20] A. J. Moses and J. Liu, "Quantification of the accuracy of different approaches to modeling anisotropy of grain-oriented electrical steel," *J. Physique IV*, vol. 8, no. 2, pp. 595–598, 1998.